Synthesis and characterization of solution-processed indophenine derivatives for function as a hole transport layer for perovskite solar cells

Shiwei Ren, Amirhossein Habibi, Pingping Ni, Hindia Nahdi, Fatima Zahra Bouanis, Sophie Bourcier, Gilles Clavier, Michel Frigoli, Abderrahim Yassar

▶ **To cite this version:**

Shiwei Ren, Amirhossein Habibi, Pingping Ni, Hindia Nahdi, Fatima Zahra Bouanis, et al.. Synthesis and characterization of solution-processed indophenine derivatives for function as a hole transport layer for perovskite solar cells. Dyes and Pigments, 2023, 213, pp.111136. 10.1016/j.dyepig.2023.111136 . hal-04287574

HAL Id: hal-04287574
https://hal.science/hal-04287574

Submitted on 16 Nov 2023

HAL is a multi-disciplinary open access archive for the deposit and dissemination of scientific research documents, whether they are published or not. The documents may come from teaching and research institutions in France or abroad, or from public or private research centers.

L'archive ouverte pluridisciplinaire **HAL**, est destinée au dépôt et à la diffusion de documents scientifiques de niveau recherche, publiés ou non, émanant des établissements d'enseignement et de recherche français ou étrangers, des laboratoires publics ou privés.

Synthesis and Characterization of Solution-Processed Indophenine Derivatives for Function as a Hole Transport Layer for Perovskite Solar Cells

Shiwei Ren[1], Amirhossein Habibi[1], Pingping Ni[1], Hindia Nahdi[1], Fatima Zahra Bouanis[1,2], Sophie Bourcier[3], Gilles Clavier[3], Michel Frigoli[4], Abderrahim Yassar[1]

1) LPICM, CNRS, Ecole Polytechnique, Institut Polytechnique de Paris, Palaiseau, 91128 France
2) COSYS-IMSE, Univ Gustave Eiffel, IFSTTAR, F-77454 Marne-la-Vallée, France
3) Laboratoire de Chimie Moléculaire, CNRS UMR 9168, École Polytechnique, Institut Polytechnique de Paris, Palaiseau, France
3) Université Paris-Saclay, ENS Paris-Saclay, CNRS, PPSM, 91190, Gif-sur-Yvette, France
4) Institut Lavoisier de Versailles, UMR CNRS 8180, University Paris-Saclay, 45 avenue des Etats-Unis, 78035 Versailles Cedex, France

Abstract

A series of quinoidal molecules were synthesized via a new variant of the indophenine reaction. The previously reported synthetic route of indophenine dyes involves a one pot procedure starting with isatin and an appropriate 5-membered aromatic heterocycle in the presence of catalytic amount of sulfuric acid. However, the reaction conditions lead to a low yield and a poor selectivity with the formation of several by-products. Herein, we propose a modification of the standard reaction to increase the yield, using tertiary alcohol as a starting material instead of isatin. This modified protocol is highly selective and allows for a very clean reaction, i.e. high yields, isomer-free synthesis and avoids any complex purification issues. Further, this protocol allows access to quinoidal compounds with variable termini and π-conjugated core. The influence of the conjugation length of the π-bridge on the quinoidal electronic structure is investigated by spectroscopic and electrochemical measurements. Meanwhile, the charge carrier mobilities of selected compounds were determined by the space-charge-limited-current method. Their utility as a hole transport material for the perovskite solar cells is demonstrated.

1. Introduction

Quinoidal systems have recently attracted much attention as a building block for the synthesis of functional conjugated materials, due to their highly planar structure which is beneficial for strong π-π stacking interactions, efficient charge transport, a high π-electron delocalisation resulting in reduced band-gap and amphoteric redox behavior which makes them potential candidates as n-type and ambipolar materials.[1-2] Among various quinoidal molecules, indophenine derivatives have received little attention, since they exist as a mixture of all six possible geometric isomers.[3] The existence of isomers would affect the ability of the molecular self-assembly to form highly crystalline thin film and thus impact the charge carrier mobility. The isomer formation is believed to occur by rotation about certain bonds in the cations, which are formed in the indophenine reaction.[3] Indeed, in standard indophenine reaction, the thiophene reacts with isatin in the presence of sulfuric acid to produce cations, and therefore coupling occurs leading to all six possible stereoisomers. Although the reaction

is simplistic, the purification of the final product is not an easy task due to the formation of isomers and the low yield of the reaction. Moreover, this reaction produces two quinoidal molecules with different core lengths, one of which is indophenine with bithiophene in 36% yield and second one is indophenine with mono-thiophene in 18% yield.[4,3] The latter, QUT in Figure 1, considered as a by-product, was isolated and characterized by a combination of 1D and 2D NOESY NMR spectroscopy analyses, and was found to be a mixture of the three isomers in the *Z, E*-configuration[4].

In addition to the classical method with sulfuric acid, an alternative method for the synthesis of indophenine dyes was developed by Ren *et al*.[5,6] This involves the Sn^{II}-mediated reductive aromatization of diol followed by oxidative dehydrogenation with 2,3-dichloro-5,6-dicyano-1,4-benzoquinone (DDQ) to produce a mixture of three isomers. To overcome the serious problem of stereochemistry, two approaches have been explored. The first method involves the oxidation of thiophene to form thiophene-S,S-dioxide which in turn induces a steric hindrance and leads to thiophene-S,S-dioxidized indophenine (IDTO) as a single pure isomer. The second is based on the use of noncovalent conformational lock and steric repulsion as a driving force for the formation of a single isomer product. Deng *et al*. found that the oxidation of thiophene ring to its 1,1-dioxides of the quinoidal bithiophene unit in indophenine molecule has a dual advantage: (i) it significantly lowers the LUMO and HOMO energy levels and (ii) it leads to the formation of a single isomer product, i.e., the (*E*,*E*,*E*)-form thiophene-S,S-dioxidized indophenine.[7] So, the oxidation of the bithiophene linker in the indophenine molecules with *m*-chlorobenzoic acid produces a mixture of three isomers (*E*,*E*,*E*), (*Z*,*E*,*E*) and (*Z*,*E*,*Z*). When this mixture is heated in toluene, only one single isomer of IDTO is observed.[8] The same approach was used to prepare thienothiophene indophenine derivatives as a mixture of six isomers.[5] By introducing oxygen atoms into thienothiophene linker, only three pure (*E*,*E*,*E*) isomers were obtained. This suggests that the oxygen atoms incorporated into the thienothiophene linker exert a steric effect to prevent the formation of other isomers. Again heating at 100 °C, affords to one single isomer (IDOTT).

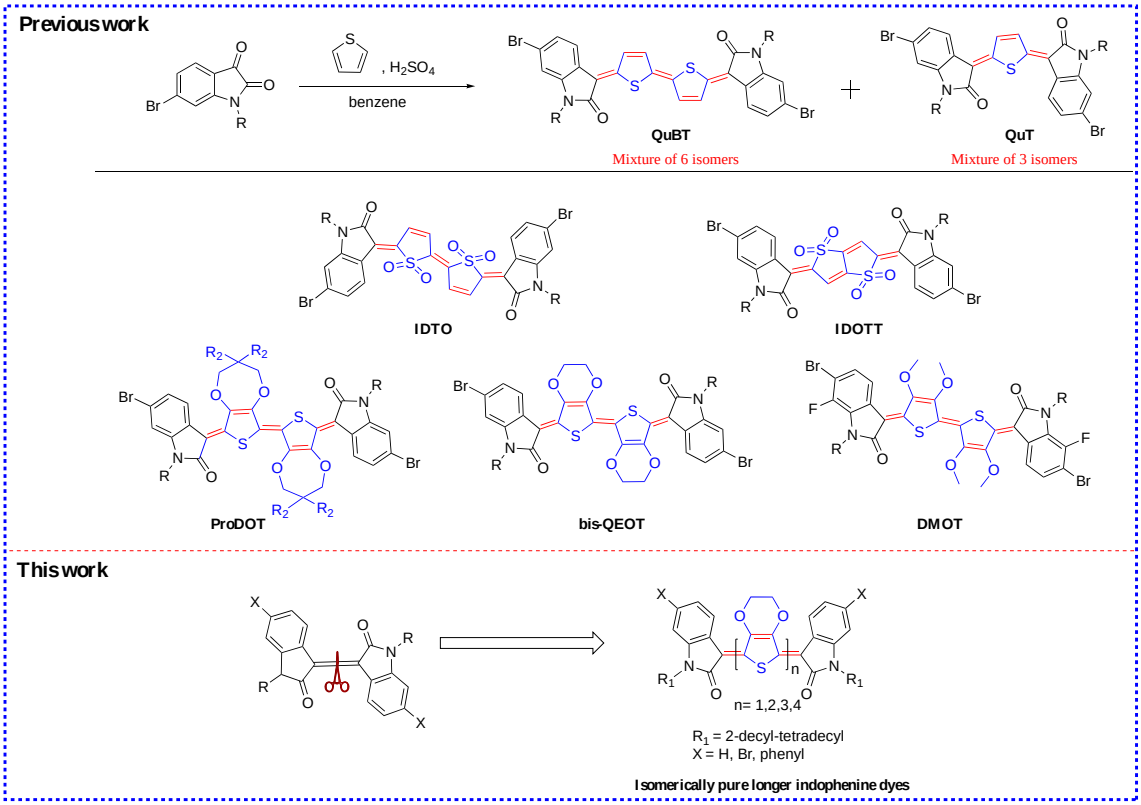

Figure **1**: Chemical structures of isomerically pure indophenine derivatives reported in the literature, and chemical structures reported in this work along with cartoon representation of the approach used for the synthesis of indophenine derivatives.

The second approach involves noncovalent conformational lock as a driving force to obtain isomer-free indophenine dye molecules. Pappenfus *et al*. were the first to propose noncovalent conformational lock, such as S....O to produce isomer-free indophenine.[9] In such approach, the intermolecular interaction between the sulfur of 3,4-propylenedioxythiophene (ProDOT) and the carbonyl oxygen of the oxindole-ring drove the reaction to single isomer formation. By following the same concept, Hwang *et al*. exploited the O···S noncovalent conformational lock to manipulate *syn*- and *anti*-isomerization of a bis-3,4-ethylenedioxythiophene indophenine.[10] As a result, a single isomer of bis-QEDOT was produced by introducing bis-3,4-ethylenedioxythiophene (EDOT) as a linker group, its geometrical structure was identified by ^{1}H NMR and density functional theory calculation. More recently, replacing a H atom with a methoxy group in the thiophene ring promotes O···S conformational locking in the backbone of quinoidal indophenine.[11] With the substitution of the methoxy group at the 3,4-position in thiophene, only a single isomer (*Z*,*E*,*Z*) was observed via a standard indophenine reaction (DMOT). The existence of O···S conformational locks has been demonstrated by solving the single-crystal structure.[9],[11] The X-ray structure of 3,4-dimethoxythiophene indophenine shows a highly planar core with a distance of only 2.69 Å between the S atom of 3,4-dimethoxythiophene and the O atom of C=O in oxindole units, smaller than the sum

of the van der Waals radii of these atoms, indicating the existence of a through-space noncovalent interaction, which leads to a quasi-perfect coplanarity between the two thiophene moieties.

Regarding the applications of indophenine dyes in organic electronics and energy devices, many studies have reported, the use of indophenine based materials as active layers in organic field effect transistor and demonstrated high charge mobility up to 3.60 $cm^2 V^{-1} s^{-1}$. [12,1] Quinoidal low band gap (LBG) material also has a major advantage when employed as a hole transport material in perovskite solar cells (PSCs), since it improves the absorption of near-infrared photons.[13] To date, a myriad of new hole transport materials (HTMs) have been synthesized and tested in PSCs,[14] however, only a few studies have been devoted to developing LBG organic materials for PSCs. The reason is that narrowing of bandgap would enhance the efficiency losses in solar cells due to the interface recombination processes.

Despite the progress made on the synthesis and the stereochemistry of quinoidal indophenine building blocks, the indophenine reaction still suffers from a low yield, the formation of isomers, and undesirable byproducts. Therefore, the development of a novel, efficient and simple method to prepare functional indophenine dyes is still desirable to produce new organic materials for energy and optoelectronic applications.

We wondered whether isomer-free of π-extended analogues of indophenine dye would be accessible based on recent progress in the synthesis of π-conjugated quinoidal molecules. Specifically, we hypothesized that a π-extension of the bridge could provide air-stable, soluble planar quinoidal molecules with a LBG energy. Along with this beneficial effect, the oxindole terminal unit can easily be functionalized by incorporating electronically neutral, donor or acceptor groups. Motivated by these synthetic challenges, we report herein a facile method with improved yields for the synthesis of isomer-free functional indophenine derivatives. We demonstrated that a modified protocol employing tertiary alcohol as a starting material instead of isatin gave a high yield with minimal purification compared to the standard conditions. This modified protocol is highly selective and allows for a very clean reaction, high yields, isomer-free materials and avoids any complex purification issues. The utility of these indophenine molecules as a hole transport material for the PSCs is demonstrated.

2. Results and discussion

2.1. Design, synthesis and characterization of indophenine derivatives

The synthetic routes to indophenine derivatives are illustrated in scheme **1**, the detailed synthetic procedures are provided in the Supporting Information (SI). To solve the solubility issue, the nitrogen atom of isatin ring was functionalized with linear or branched alkyl chains. To further derivatize the indophenine molecules, 6-bromo-isatin was also used as starting block which was synthesized through a two-step procedure, known as Sandmeyer reaction, starting from 3-bromoaniline.[15] Two synthetic strategies were employed to obtain functional indophenine dyes with different conjugated π-bridges (i.e., the mono-EDOT for **3a**, **3b**, **3c** and **3b'**, bis-EDOT for **5a**, **5a'**, **5b'** and **5c**, ter-EDOT for **9a** and **9a'** and quater-EDOT for **11a'**). The first route involves the formation of

diols followed by a reduction reaction using $SnCl_2$ and subsequent oxidation with DDQ.[16-17] The second relies on the dehydrating dimerization of easily accessible tertiary alcohols, via delocalized carbocation intermediates.

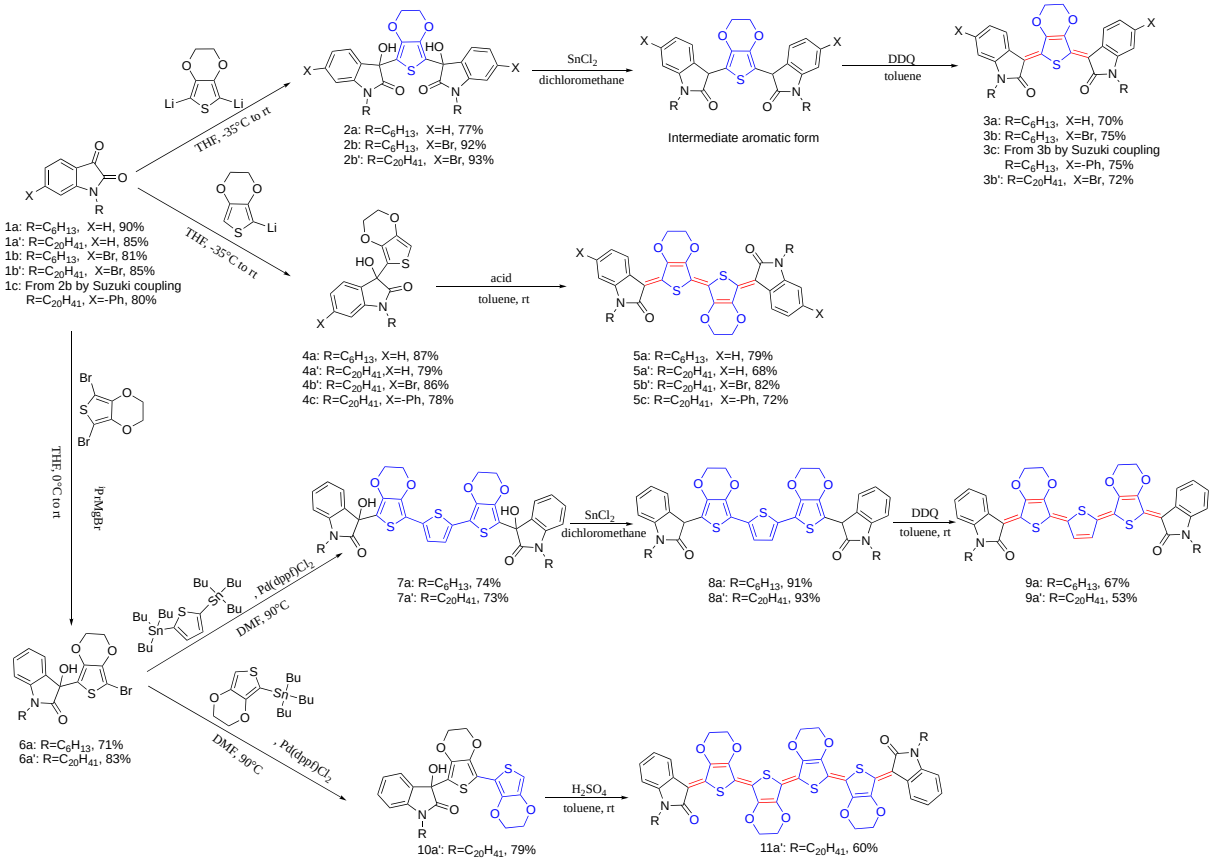

Scheme 1. Synthetic routes of isomer-free indophenine dyes.

The first strategy was applied to prepare compounds containing an odd number of rings, while the second approach is used to prepare compounds with an even number of rings (Scheme 1). Mono-EDOT derivatives (**3a-c)** were obtained in three steps from isatin derivatives. EDOT was treated with *n*-BuLi at -78 °C in THF and the resulting doubly lithiated EDOT was reacted with isatin derivatives to give the diol intermediates **2a-b** and **2b'** as diastereomeric mixtures in yield equal or superior than 77 %. The splitting pattern and chemical shift of the protons of the N-CH_2 in aliphatic chain (H_f) of **2a** indicates the presence of *cis-trans* diastereosiomers in a ratio 1:1 (Figure S1 in SI). Subsequent reduction of the resulting diols with $SnCl_2$ gave the corresponding hydrogenated intermediates, which can be readily transformed to the target quinoidal compounds using DDQ, in yields up to 70%. The structures of **3a-c** were fully verified by ^1H, ^{13}C NMR, IR, and HRMS. The ^1H NMR spectra show the formation of a single isomer. For instance, the ^1H NMR spectrum of **3b**, shows three different proton peaks with identical integral ratios in the aromatic region, one singlet at 4.6 ppm for ethoxy and one triplet at 3.63 ppm for N-CH_2 (H_e), Figure S2. This indicates that the structure of **3b** is symmetrical with respect to the EDOT moiety. The H_a proton has the most downfield signal (8.01 ppm) owing to

the large deshielding effect caused by an intramolecular hydrogen bonding interaction between the H_a and the oxygen atom of EDOT indicating that the carbonyl function points to the sulfur atom. Further functionalization of compound **3b** was performed via Suzuki-Miyaura cross-coupling reaction and afforded the phenyl derivative **3c**.[18-19]

Considering that the formation of the quinoidal compounds from diol precursors works well, the terthiophene derivatives were obtained from diol intermediates **7a**,**a'** which were obtained in two steps from isatin derivatives **1a,a'**. First, the mono-Grignard reagent of 2,5-dibromo-EDOT, obtained by Grignard exchange reaction between dibromo-EDOT and *i*-PrMgBr was reacted with isatin derivatives **1a,a'** to produce alcohol-EDOT **6a,a'**.[20] Then, the latter underwent palladium-catalyzed cross-coupling reaction with 2,5-bis(tributylstannyl)thiophene to give compound **7a,a'** in yield about 70%. Reductive elimination of diols **7a**,**a'** using $SnCl_2$ under acidic conditions, followed by the oxidation with DDQ afforded the final compounds **9a,a'** in good yield as a dark blue powder. The structure of **9a'** was characterized by using ^{1}H NMR and high-resolution mass spectrometry (HRMS) (Figures S3 and S4). The HR-APPI-MS spectrum of **9a'** clearly shows an intense signal at m/z 1185.6816 uma for the molecular protonated ion $[MH]^+$, corresponding to the targeted compound. As for mono-EDOT derivatives; only one isomer was produced for which both carbonyls point to the sulfur atom because the proton Ha is most deshielded. (Figure S3).

The second strategy employed to prepare indophenine dyes with a bis-EDOT as a linker, is based upon Cava's condition.[3] However, the reaction conditions lead to a poor yield with a low selectivity along with the formation of isomeric mixtures that are difficult to separate. Inspired by this work, we proposed a modification of the conditions of the conventional reaction to increase the yield, using tertiary alcohol as a starting material. The key alcohol derivatives **4a, a', b'** and **4c** were prepared in good yields (78-87%), by the addition of mono-lithiated-EDOT to isatin at -35°C. The resulting mixture of both *cis* and *trans* diastereomers in 1:1 ratio, was used without further purification for the next step. We hypothesized that a strong acid would lead to the formation of cation, via delocalized carbocation, which in turn attacks the α-position of the EDOT ring of a second molecule to form a dimer, via formal elimination of water, scheme S1. Two types of acids were used, the first is concentrated sulfuric acid and the second is an organic acid p-toluenesulfonic acid. When a catalytic amount of sulfuric acid was used an excellent yield, 75% of **5a** was obtained. The p-toluenesulfonic acid-catalyzed reaction also yielded to the target product with 55% yield. The structure of **5a**,**a'**,**b'** were verified by ^{1}H NMR, ^{13}C NMR, and HRMS. With the help of ^{1}H NMR experiments, ^{1}H–^{1}H COSY and ^{1}H-^{1}H NOESY analyses, we confirmed a single isomer formation. For instance, in the ^{1}H NMR spectra of **5a'**, the symmetrical peak shape belonging to the CH_2 of the EDOT ring near 4.5 ppm not only indicates a symmetrical molecular structure but also proves the formation of single isomer, Figure S5.. The two double peaks at 8.18 and 6.72 ppm correspond to H_a and H_d respectively,. The other two triplet peaks were accurately assigned using ^{1}H-^{1}H COSY NMR, Figure S6. While 2-bond

and 3-bond ^{1}H-^{1}H coupling is easily visible by COSY, long range coupling can also be observed with long acquisition times.[21]

To better understand the structural information of **5a'**, we carried out ^{1}H-^{1}H NOESY measurements. We found that the ^{1}H-^{1}H NOESY spectrum of **5a'** showed three strong cross-peaks labeled 5-7, which are not founded in the COSY spectrum, Figure S7. The cross-peaks in ^{1}H-^{1}H NOESY indicate the concerned nuclei are spatially close. In this case, cross-peak, labeled 5, suggest that the proton H_a at 4-position of oxindole is spatially close to H_e of EDOT. Cross-peaks labeled 6 and 7 indicate H_d of oxindole is also spatially close to the protons at H_g and H_h of the alkyl chain. Therefore, we can propose *cis-trans* configuration of the Bis-EDOT rings, namely the sulfur atom is directed toward the carbonyl group of oxindole, as shown in the inset of Figure S5. This is consistent with previous findings from X-ray structural studies.[9] More importantly, the excellent solubility of **5a'** allowed for a concentration-demanding ^{13}C-NMR spectrum with a high signal/noise ratio, Figure S8. ^{13}C NMR confirms again that the **5a'** is an isomer-free molecule and to our best knowledge, this is the first report of ^{13}C NMR of the indophenine-EDOT derivatives. Although this indophenine derivative was early reported, but no ^{13}C NMR spectrum was reported due to the solubility issue.[22],[9],[10] An accurate assignment of ^{13}C-NMR spectra of **5a'** was obtained thanks to the combination of ^{13}C NMR and DEPT 135, Figure S8.

The selectivity of this modified protocol was further investigated. To this, we prepared the alcohol intermediate **4c** with a phenyl group on the peripheral position of the isatin. In this intermediate, there are two susceptible oxidation sites: the phenyl on the isatin side and the EDOT ring. Under the condition of catalytic amount of sulfuric acid, the product of the dimerization of the EDOT, product **5c**, was regioselectivity synthesized. The benzene ring at 6-position was not attacked and oxidized by sulfuric acid. The molecular structure of **5c** was confirmed by ^{1}H, ^{13}C NMR, IR, and HRMS. The average yield of this modified reaction (**5a,a',b',c**) is 75% which is much higher than the yield of standard reaction condition previously reported.[8] It is worth mentioning that under standard condition the yield is about 20% [3] and the formation of indophenine with mono-thiophene as a by-product cannot be avoided. However, in our conditions the reaction shows a high selectivity, without the formation of a by-product. This high selectivity is an advantage as it allows for a very clean reaction, isomer-free synthesis and avoids any complex purification issues. Encouraged by this result, the scope of the new variant of the indophenine reaction with regard to bis-EDOT was then examined to synthesise indophenine with four EDOTs as a π-bridge. Stille coupling[23] reaction of **6a'** with 2-tributylstannyl-3,4-ethylenedioxythiophene affords to the intermediate **10a',** which has two EDOT units. Upon the addition of a catalytic amount of sulfuric acid, a large amount of solid precipitates and the solution becomes dark blue. The structure of **11a'** was confirmed by ^{1}H NMR, and HRMS (see Figures S9 and S10).

2.2. Optical, electrochemical and electrical properties of indophenine derivatives

Theoretical calculation

To understand the trend in the HOMO−LUMO energy levels and band gaps of indophenine materials we carried out theoretical calculations to investigate molecular structure-optical properties relationships. The calculations were performed by using density functional theory (DFT) at the PBE0/6-311+g(d,p)//CAM-B3LYP/6-31+g(d) level of theory including dichloromethane solvent effect (iefpcm formalism). The time dependent density functional theory (TD-DFT) has been applied to calculate the vertical transitions (PBE0/6-311+g(d,p) level of theory). In all of the indophenine derivatives the longer alkyl chains were replaced by butyl groups to reduce computational cost.

The fully optimized structures of stable isomers are shown in Fig. S11. The computed geometrical parameters of **3a**, **3b'**, **5a'**, **5c**, **9a'** and **11a'** are compiled in Table S1. The influence of the S···O interactions on the stable conformation of each isomer was assessed by comparing the total energy of the three isomers of **3a** where the S atom in EDOT ring is situated close to or away from the oxygen of the carbonyl group (Figure S12). Isomer **1** is flat but upon rotation of the oxindole unit it is out of the plane of the EDOT by ≈12°. The energy of isomer **1** is 4.64 kcal/mol lower than that of isomer **2** and 11.23 kcal/mol lower than that of isomer **3** which is consistent with the stabilizing effect brought about by the S···O interactions as previously observed in single crystal.[9] The dihedral angle between the oxindole ring and the EDOT moiety is close to 2° indicating a nearly planar structure. While a dihedral angle of 39° between the plane of the phenyl ring and oxindole group is observed in **3c** and **5c**, suggesting a limited delocalization of π-electrons over the whole molecular skeleton. The theoretically estimated HOMO (LUMO) energy level and band gap values of **3a**, **3b'**, **5a'**, **5c**, **9a'** and **11a'** are listed in table S1. The theoretically calculated band gap decreases from 2.77 eV for **3a** to 1.63 eV for **11a'**. As the number of EDOT units increases in the π-bridge linker, the energy of HOMO decreases while the LUMO energy remains relatively unchanged, giving a reduced band gap. The substitution of hydrogen atom in the oxindole group with a phenyl ring, compound **3c**, led to a decrease of the HOMO energy level to -5.71eV. The theoretically calculated HOMO, LUMO energy levels and band gaps are in close agreement with experimental data, electrochemical and optical results, as will be discussed in next subsections. The plots of frontier orbitals indicate that the HOMO is delocalized over the entire molecule, while the LUMO is more localized on the π- bridge which differs from the dicyano quinoidal oligothiophene where the terminal electron-withdrawing $C(CN)_2$ groups equally participate in both FMOs and lowering the energy levels of the LUMO, Figure S13-S14. The bond-length alternation (BLA) is used to assess the geometrical variations. A quinoidal ring is characterized by a negative BLA value, while an aromatic ring has a positive BLA value. All of the above structures show a C=C double- bond length of EDOT ring and inter-ring C=C bond length close to 1.36 Å. In compound **3a**, EDOT ring shows a BLA value of −0.096 (Å), whereas compound **11a'** show a BLA value of −0.075 (Å). The increase of the conjugation length of the π-bridge causes a decrease of BLA value, Figure S16. This could be explained by the fact that **11a'** exhibits a stronger aromatic character. Table S1 lists the computed energy of the electronic transitions and optical band

gaps for all the compounds. From this result, it can be observed that the first electronic transition is occurring from the HOMO to LUMO in all compounds.

Optical characterization

The chain-length-dependent optical properties of indophenine derivatives were investigated by UV-Vis spectroscopy in dilute dichloromethane (DCM) solutions, Figure 2 and Figure S17 a-f. All compounds show one main band, with a shoulder at each side of the absorption maximum (λ_{max}). The shoulder is assigned to the vibronic structure, which is usually observed in quinoidal oligomers.[24] In **3a** the main absorption band appears at 473 nm and the shoulders at 444 nm and 531 nm. This absorption band shifted to lower energy, became broad and lost structure as the number of EDOT units increases from mono-EDOT (473 nm) to tetra-EDOT (820 nm). These intense bands are mainly assigned to the HOMO–LUMO transition as demonstrated in the previous section. Furthermore, the molar extinction coefficients were found to increase with increasing number of EDOT units from 1 (ε = 24728 M^{-1} cm^{-1}) to 2 (ε = 96932 M^{-1} cm^{-1}). Molar extinction coefficients for longer dyes could not be accurately determined, due to the strong tendency of the dyes to aggregate in solutions.

As a general trend, a strong regularity of bathochromic shift of the λ_{max} assigned to the π-π^* (HOMO→LUMO) transition of the conjugated π-system is observed with the extension of the π-bridge, confirming full conjugation of the π-system. The maximum absorption band exhibits an average redshift of 114 nm with the addition of one EDOT unit, Figure S18. This wavelength maxima behavior is similar to those of the tetra-cyano quinoidal oligothiophenes[25], but they are red-shifted, likely due to the influence of the oxindole units on the delocalization and energy of the frontier orbitals. The π-bridge length-dependent evolution of the energies of the band maxima (λ_{max}) is represented in Figure S18, together with those λ_{max} values of tetracyano quinoidal oligothiophenes, from a mono- to a hexa-thiophene. For both series of quinoidal compounds, the evolution of λ_{max} versus 1/n displays two linear regions, with the quaterthiophene structure placed at the tuning point of the two linear fits. This behavior has been explained by accounting of the formation in quaterthiophene structure a broken double bond of the full quinoidal form which allows the aromatization of the thiophene rings, which means that mixed aromatic and quinonoid units coexist in the same structure and the formation of a diradical system.[26] The optical band gaps estimated from the onsets in the absorption spectra are found to be, 1.96 eV for the compound **3a**; 1.85 eV for compound **3b'**; 1.3 eV for compound for **9a'** and 1.18 eV for compound **11a'**.

Regarding the effect of the substituents on the terminal oxindole ring, introducing a bromine atom at the 6,6'-position has a small red shift effect on the maximum of the absorption peak and reduced the optical band gap. While substituting a benzene ring at 6,6' position of the oxindole, produces a red shift of about 100 nm for phenyl derivative mono-EDOT, compound **3b'** shows a spectrum with a λ_{max} of 575 nm, compared with that of compound **3a** (473 nm); and 30 nm red-shift for phenyl derivative bis-EDOT, compound **5c** has a λ_{max} of 661 nm which is slightly red-shifted compared to **5a'** (633 nm), Figure S17 **a** and **f**.

The overall result is that, one can fine tune the optical properties and band gap energy of indophenine dyes by carefully controlling either the conjugation lenght of the π-bridge linker unit or the substituents at the terminal oxindole units.

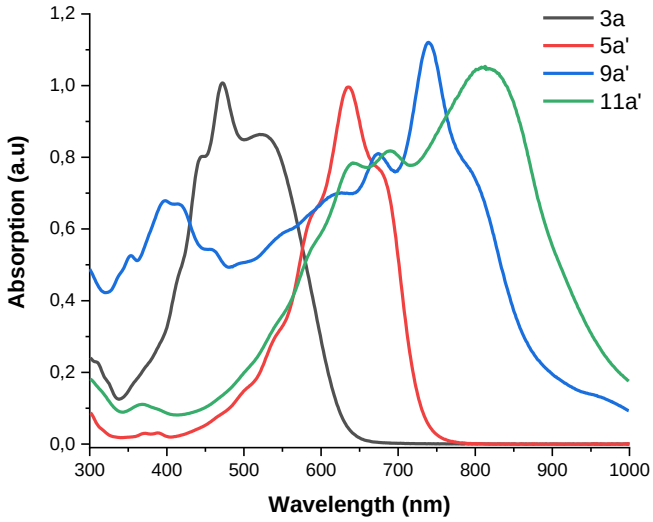

Figure 2. Normalized solution UV-vis-NIR absorption spectra of indophenine dyes in DCM.

Electrochemical characterization

For studying the energies of electronic levels in organic semiconductors, several methods are more appropriate such as, the photoelectron spectroscopy techniques: Ultraviolet photoelectron spectroscopy,[27] inverse photoelectron spectroscopy (for LUMO),[28] photoelectron yield spectroscopy (for HOMO),[29] and cyclic voltammetry (CV) (for HOMO and LUMO).[30] CV has been widely used in characterization of newly organic semiconductors. However, for CV, determining peak positions of redox waves can be compromised when peaks are broad and ill-defined due to the lack of electrochemical reversibility and a large current of double-layer capacitance. Square wave voltammetry (SWV) is an alternative to CV and it is a sensitive and more suitable electrochemical technique to analyze Faradaic current while minimizing contributions from capacitive currents.[31] Recent work has shown that SWV provides a better estimation of the oxidation and reduction potentials of the organic semiconductors in thin films and the levels of the HOMO and LUMO.[32] The electrochemical properties of compound **3a** and **5a'** were investigated by solution CV and SWV methods, Figure **3** and **S19**. The HOMO and LUMO energy levels of these quinoidal compounds were estimated from the equations E_{HOMO} = -Eox -4.8 and E_{LUMO} = -E_{red} -4.8 and compiled in Table 1. All indophenine derivatives showed an amphoteric behavior, which is typical of quinoidal molecules. They undergo reversible electron oxidation to the radical cation and reduction to the radical anion, indicating that the radical cation/radical anion species are well stabilized by the quinoidal skeleton. The oxidation/reduction processes are a monoelectronic step in contrast with tetracyano quinoidal oligothiophenes (n-TQ), which display two-electron reduction waves.[33] All derivatives, **3a**, **3b'**, **5a'** and **5c** exhibit one reversible electron reduction peak at -1.39 V that is negatively shifted compared to

those of n-TQ analogues, TQ-1: -0.53 V and TQ-2: -0.65 V. This result indicates that the formation of anionic species is both kinetically and thermodynamically less stable due to the electron donating character of oxindole end-group compared to the strong electron accepting character of dicyanomethylene group.[25] As shown in Fig. 3 and Fig S19, the cyclic voltammograms and square wave voltammograms of **3a** and **5a'** exhibit one electron oxidation process. The oxidation potentials measured decrease as the π−conjugation length of the central core increase, from 0.6 V for Mono-EDOT to 0.35 V for Bis-EDOT. Compared to the HOMO level, the LUMO level is less influenced by the conjugation length of the central π-bridge, indicating that the band-gap reduction is mainly caused by the increase of HOMO level as the π conjugation extends over all indophenine unit. Whereas alkyl chain length does not affect the electrochemical behavior, both compounds **5a** and **5a'** exhibit identical HOMO/LUMO energy levels, suggesting that the influence of the alkyl chains on the HOMO/LUMO energy level is negligible. The energy level of frontier molecular orbital can also be significantly modulated by introducing substituents on the terminal oxindole block. Introducing a phenyl substituent on the oxindole terminal group lower the oxidation potential of **3b'** and **5c** by approximately 0.25 V relative to **3a** and **5a'** respectively. While the reduction peak potential remains almost unchanged upon substitution in the oxindole terminal group.

Clearly, the electrochemical properties of the indophenine derivatives, mainly the HOMO energy level could be finely tuned by modifying the central core and the oxindole end-group, which is distinct from the tetracyano quinoidal oligothiophenes, where the molecular orbital energy levels can only be tuned by manipulating the central core.

Table 1. Electrochemical data of indophenine derivatives

Compound	$\mathbf{E_{pc}}$ **(V)**	$\mathbf{E_{pa}}$ **(V)**	$\mathbf{E_{ox,onset}}$ **(V)**	$\mathbf{E_{red,onset}}$ **(V)**	$\mathbf{E_{HOMO}}$ **(eV)**[a]	$\mathbf{E_{LUMO}}$ **(eV)**[b]	$\mathbf{\Delta E^{elec}}$ **(eV)**
3a	-1.36	0.60	0.60	-1.36	-5.4	-3.44	1.96
3b'	-1.39	0.35	0.25	-1.35	-5.15	-3.41	1.60
5a'	-1.41	0.30	0.15	-1.40	-5.1	-3.39	1.55
5c	-1.40	0.05	-0.01	-1.38	-4.85	-3.4	1.37

Electrochemical Energy levels are estimated from equations from: E_{HOMO} = -(Eox + 4.8) eV. E_{LUMO}= -(Ered + 4.8), where Eox and Ered were determined from oxidation and reduction peaks of SWV respectively. Electrochemical band gap: $E_{HOMO} - E_{LUMO}$.

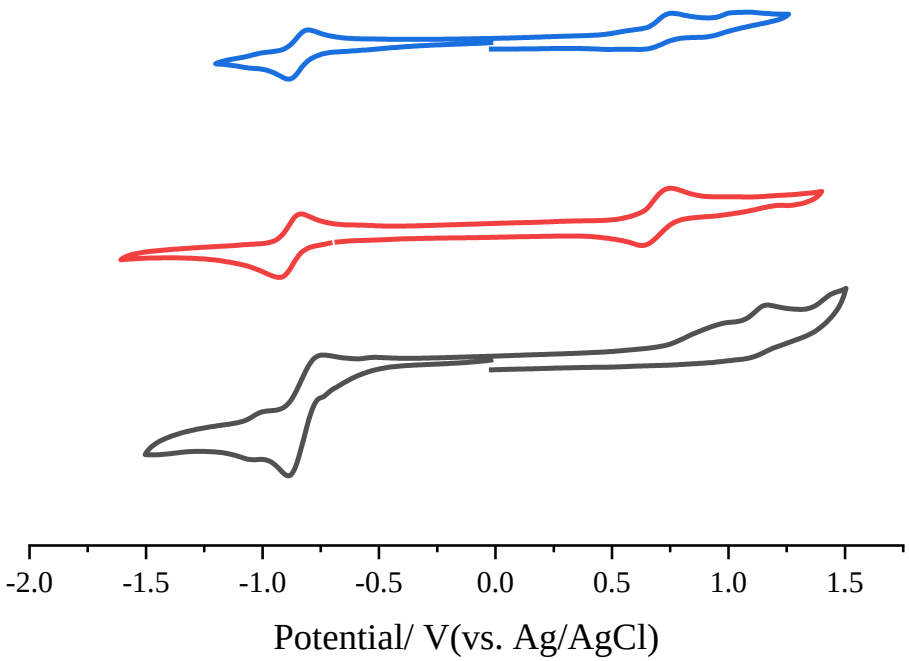

Figure **3**. Cyclic Voltammetry of indophenine dyes in dichloromethane: compound **3a** (black:); compound **5a'** (red) and compound **5c** (blue).

Electrical characterization

To demonstrate the utility of the new indophenine derivatives as a hole transport layer (HTL) for PSCs, we have chosen to focus on **5a'** and **3a**, owing to their high mobility[10],[4] and good processability. Doping is widely used as a strategy to modify the opto-electronic properties of charge transport layers in photovoltaic devices.[34] To assess charge-carrier mobilities of pristine and doped **5a'** thin films, we fabricated hole-only devices with a configuration of ITO/poly(3,4-ethylene dioxythiophene): poly(styrene sulfonate) (PEDOT:PSS)/**5a'**/Au, and we performed space-charge-limited-current (SCLC) measurements, as shown in Figure 4. The mobilities were calculated using the Mott–Gurney equation from SCLC regime. The hole mobilities were determined to be 2.8×10^{-3}, 2×10^{-3}, and 4.7×10^{-3} $cm^2\ V^{-1}\ s^{-1}$, for **3a**, pristine and doped film of **5a'** respectively. These mobility values are consistent with N-dodecyl substituted indophenine mobility values reported in the literature.[35] This result indicates that both pristine and doped films can efficiently perform as a HTL in PSCs.

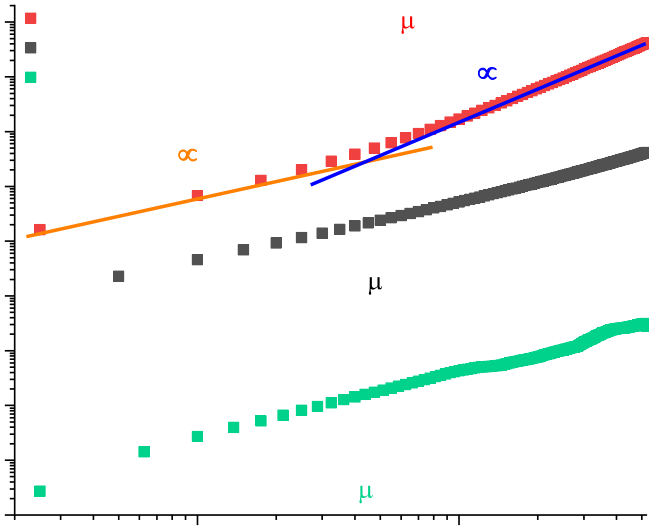

Figure 4. Current–density–voltage (J–V) characteristic of an hole-only device with structures of **5a'** (red) and **5a'**+F4TCNQ (black) and **3a** (green).

2.3. Photovoltaic performance

To evaluate the potential use of indophenine dyes as a HTL in PSCs, we compared photovoltaic (PV) performance of both indophenine molecules pristine and F4TCNQ doped film, in a conventional n–i–p structure, shown in Figure 5. The n–i–p structures were fabricated on a fluorine-doped tin oxide and titanium dioxide FTO/c-TiO_2/m-TiO_2 purchased from Solaronix (15 Ω/sq, 2×2.5 cm^2). The substrates were sintered at 450 °C for 30 min to transform completely into the rutile phase. After cooling down to room temperature, the triple-cation perovskite $(MA_{0.17}FA_{0.83})_{0.95}Cs_{0.05}Pb(I_{0.83}Br_{0.17})_3$ precursor layer was deposited on TiO_2. Then the HTL was spin coated on the perovskite layer followed by thermal deposition of gold, top electrode.

a) **b)**

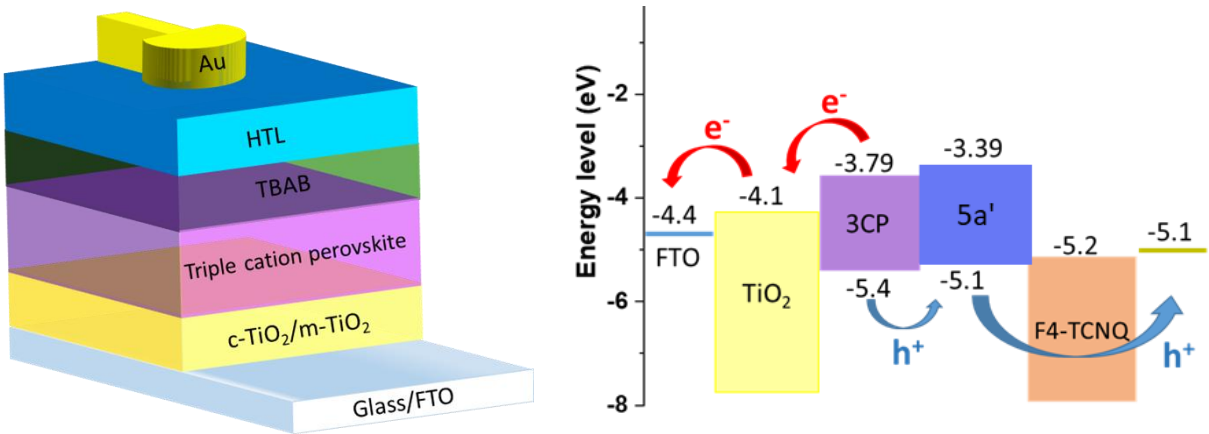

Figure 5. Device structure of the n-i-p PSC (a). Energy level diagram of the components of the n-i-p PSC (b).

We first characterized the surface morphology and optical properties of the perovskite layer. Figure 6a displays the top-view SEM of the perovskite layer deposited on m-TiO_2. The perovskite layer exhibits large grains with uniform grain size in the 300-400 nm range. The perovskite film coated on the glass substrate exhibits good light harvesting capability from the visible spectrum with ~90% light absorption with an absorption onset at 769 nm and the strongest absorption at 500–800 nm, Figure S20. Before investigating the effects of the HTLs on the device performance, we characterized the morphological and optical properties of pristine and F4-TCNQ doped films of HTL. Atomic force microscopy (AFM) examinations revealed that both pristine and doped film showed a uniform topography, as shown in Figure 6c and Figure 6d. AFM root-mean-square surface roughness of the pristine **5a'** and F4-TCNQ doped **5a'** films are 1.7 and 2.7 nm, respectively, demonstrating that the F4-TCNQ as a dopant does not modify surface morphology of HTL, which is more beneficial to enhance ohmic contact between layers and then to improve device performance. Further, the hydrophobic nature of F4-TCNQ will contribute to produce a better morphology of the photoactive layer, as we will demonstrate later.

a) **b)**

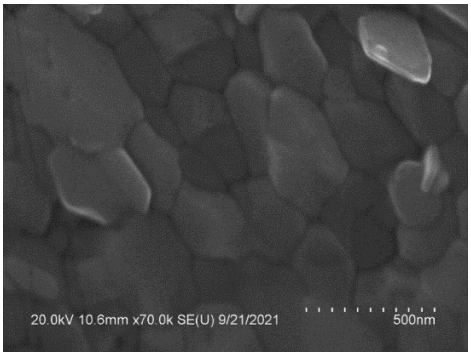

c) d)

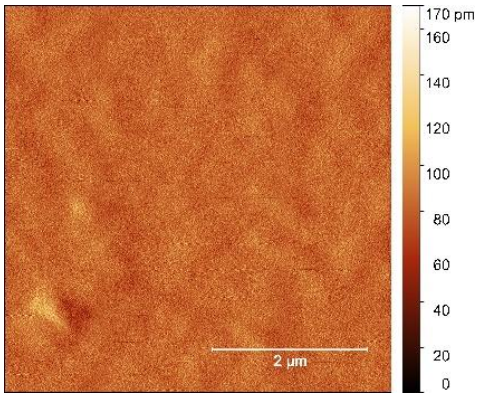

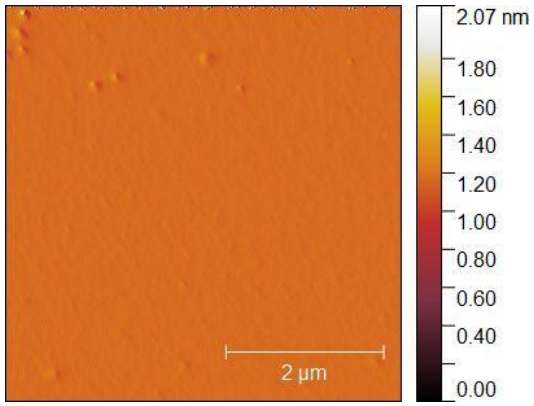

e)

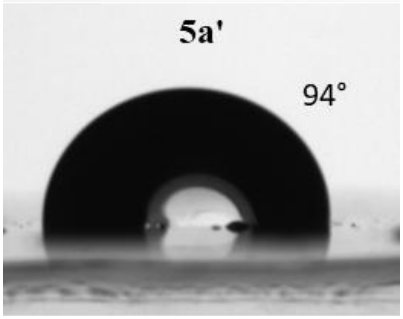

f)

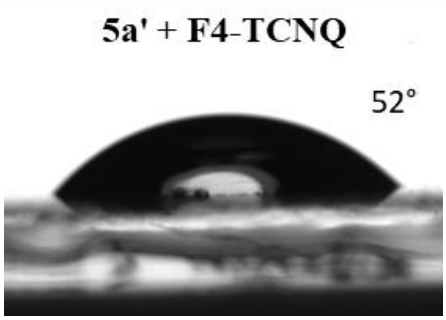

Figure 6. Top view SEM image of perovskite surface (a) cross-sectional SEM image of the perovskite solar cell device (b). AFM image of **5a'** on glass substrate (c) and **5a'** + F4-TCNQ on glass substrate (d). The water contact angel of **5a'** (e), and **5a'**+F4-TCNQ (f).

When a thin film of **5a'** layer is deposited on top of the perovskite layer, the **5a'** film does not uniformly cover the entire surface of the perovskite film, as clearly shown by confocal microscopy images, in Figure S21. This is due to the hydrophobic nature of **5a'** as demonstrated by contact angle measurements, thus, the wettability of these surfaces was evaluated by measuring water contact angles on glass substrates coated with **5a'** and **5a'** doped F4-TCNQ (Figure 6e). Film of **5a'** +F4-TCNQ is less hydrophilic, with a correspondingly low contact angle of 52 °, whereas **5a'** is hydrophobic with a contact angle of 94°. The hydrophobic **5a'** is less hydrophobic in the oxidized state than in the neutral state, this is consistent with previous studies showing a change in the contact angle between P3HT surface upon electrochemical doping−dedoping.[36] To overcome this issue, an interfacial layer of the tetrabutylammonium bromide (TBAB, 5 mg/mL in isopropanol) was spin coated onto the perovskite layer. When TBAB is used as a passivation layer, an homogenous, pinhole-free **5a'** thin film is obtained, as seen by confocal optical microscopy, Figure S21-b. Further confirmation of this point is provided by cross-sectional SEM investigations. Figure 6b displays a cross-sectional SEM image of the completed device (FTO/c-TiO_2/m-TiO_2/perovskite/TBABr/**5a'**/Au), showing that **5a'** HTL has a uniform thickness. All these observations confirm a successful deposition of a homogenous and high quality film of **5a'**, accompanied by surface smoothening of the perovskite due to **5a'** solution filling.

The hole extraction ability of **5a'** was assessed by steady-state photoluminescence (PL) measurements. PL measurements were performed on freshly prepared complete devices. As shown in Figure S22, a broad PL peak of pristine perovskite film is observed at 771 nm; while in the presence of **5a'** and **5a'**+F4-TCNQ, significant PL quenching occurs, meaning that the new **5a'** has a good hole extraction capacity. Notably, the PL intensity of the perovskite/**5a'**+F4-TCNQ has a more pronounced quenching effect, suggesting that **5a'**+F4-TCNQ could more effectively extract holes from the perovskite material.

The current density–voltage (J–V) characteristics curves of the four different HTL-based PSC devices measured under AM 1.5G simulated illumination are displayed in Figure 7 and PV parameters (PCE, power conversion efficiency; V_{OC}, open circuit voltage; FF, fill factor; and J_{SC}, short-circuit current) extracted from the J−V curves are summarized in Table 2 and the statistical results in Figure 9.

The control device using P3HT as an HTL shows a PCE of 8.14%, with a V_{OC} of 0.85 V, a J_{SC} of 15.73 mA.cm$^{-2,}$ and a FF of 60.6%. According to the statistical results, the PSCs with **5a'** showed the lowest performance with a V_{OC} of 0.74 V, a J_{SC} of 12.31 mA.cm^{-2}, a FF of 40%, and an overall PCE of 3.67%. Meanwhile, devices with TBAB/**5a'** showed better performance (V_{OC} = 0.88 V, J_{SC} = 18.60 mA.cm^{-2} and FF = 47% for the best device), resulting in efficiencies of about 7.5%. The best performance was obtained from TBAB/**5a'**+F4-TCNQ, with a V_{OC} of 0.84 V, a J_{SC} of 21.05 mA.cm^{-2}, a FF of 52%, and an efficiency of 9.17% for the champion cell. The enhanced performance is due to a better hole-extracting capability of the doped **5a'** and the uniform covering of the perovskite surface. The latter was assessed by surface wettability measurements of F4-TCNQ-doped thin films, shown in Figure 6f. The doped film is found to have a hydrophilic surface with a water contact angle of 52° which is beneficial for achieving good covering of photoactive layer.

Table 2. The PV parameters of the device performance (champion cell for each structure).

Type of HTLs	V_{OC} (V)	J_{SC} (mA cm^{-2})	FF (%)	PCE (%)
P 3HT (as reference)	0.85	15.73	60	8.14
3CP/**5a'**	0.74	12.31	40	3.67
TBAB/**5a'**	0.88	18.60	47	7.72
TBAB/**5a'**+ F4-TCNQ	0.84	21.05	52	9.17
TBAB/**3a**	0.93	13.56	53	6.66

Surprisingly, the J_{SC} of **5a'**-based cells was comparable to those obtained from P3HT-based devices despite low FF and V_{OC}. The reason for the increased J_{SC} can be interpreted as the efficient hole extraction capability owing to the high hole mobility of **5a'**. On the other hand, V_{OC} and FF losses

could be attributed to the increased series resistance and reduced shunt resistance associated with the interfacial carrier recombination kinetics that occurred between perovskite and HTM layer owing to the misalignment between the perovskite and the transport layer. Even if the mobility of **5a'** is similar to literature values of P3HT, determined by SCLC measurements, $\mu \approx 2.8 \times 10^{-4}$ cm^2 V^{-1} s^{-1},[37] it is possible that the carrier concentration is low, which would result in poor conductivity. Thus, F4-TCNQ doped HTL exhibits a significant enhancement of the J_{SC} up to 21.05 mA cm^{-2}, and a moderate value of FF (52%). The other reason for the low FF and V_{OC} is the recombination at the TiO_2/HTM interface as suggested by Palomares et al. [38] They investigated the charge recombination kinetics using transient photovoltage and laser transient absorption spectroscopy in $MAPbI_{3-x}Cl_x$ PSCs using LBG polymers as HTM. Their results clearly assigned both transient photovoltage and absorption spectroscopy decays to the recombination process between photo-injected electrons in TiO_2 and the holes in HTL. To analyze the influence of the recombination at the perovskite/TiO_2 interface, we fabricated devices incorporating phenyl-C_{61}-butyric acid methyl ester (PCBM) or LiTFSI in TiO_2. Devices with TiO_2/PCBM and TiO_2/LiTFSI exhibited better PV performance due to the better Voc and FF, Figure S23 and table S2. This underlines the effect of interfacial recombination of charge carriers and charge accumulation at the interface between the TiO_2 and the perovskite active layer.

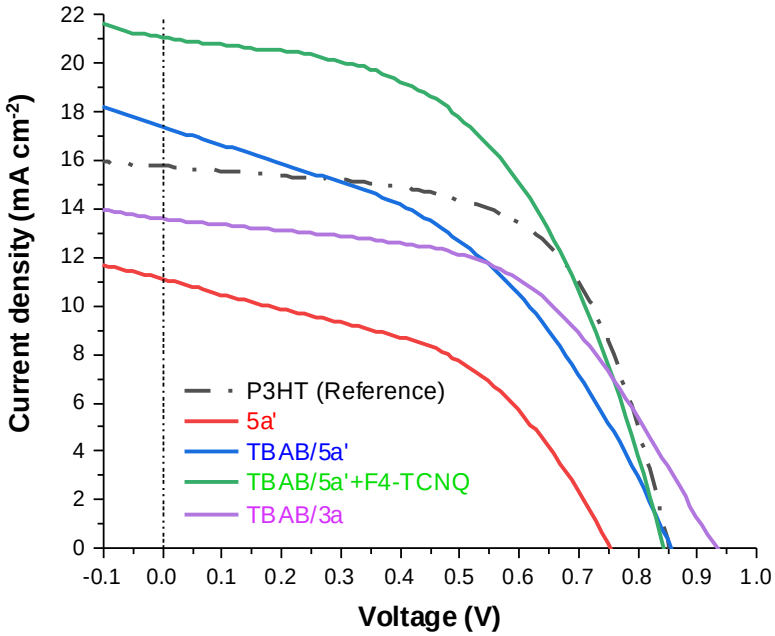

Figure 7 Current density–voltage curves for the best-performing PSC devices (a).

To validate the hole transport functionality of **3a**, we made a n-i-p PSC device, FTO/c-TiO_2/m-TiO_2/perovskite/TBAB/**3a**/Au, of which we measured the J−V characteristics under AM1.5G illumination. Figure 8b displays the surface morphology of **3a** thin film. The surface of **3a** was smooth, pin-hole free and the root-mean-square was estimated to be 3.25 nm. This result suggests a good film formation ability of this molecule, which is important to prevent current leakage and facilitate better charge career efficiency in the PSCs, as shown by a cross-sectional SEM image, Fig

8a. This device structure delivers a normal J−V curve of a typical n-i-p PSC device with a V_{OC} of 0.93 V, a J_{SC} of 13.56 mA.cm^{-2}, a FF of 53%, and a PCE of 6.7 %. The lower efficiencies of these devices compared to those the TBAB/**5a'** devices are mainly driven from the drop of J_{SC} (18 mA.cm^{-2} on average for TBAB/**5a'** devices), even if TBAB/**3a** cells have shown better V_{OC} and FF.

a) **b)**

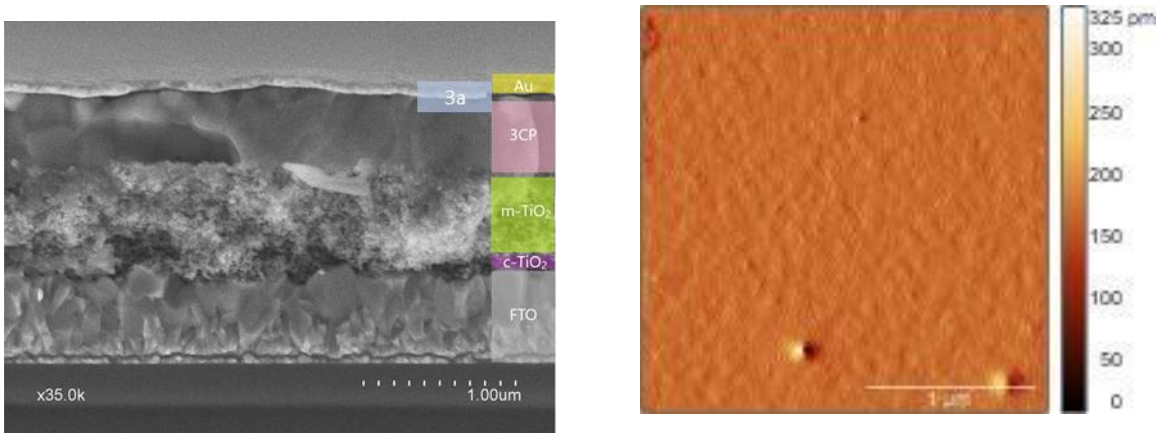

Figure 8. Cross-sectional SEM image of FTO/c-TiO_2/m-TiO_2/perovskite/TBAB/**3a**/Au device, (a) and AFM image of **3a** (b).

To provide a better insight, we compare our results to those reported in the literature employing a LBG HTM, Table S3. Firstly, it should be underlined that the best PCE of 10% achieved, when employing **5a'** as HTL, is among the best reported in the literature for LBG HTMs, although slightly lower than that of the donor-acceptor copolymers. The maximum PCE values reported for PSCs employing LBG hole transport materials were, in fact, lower compared to those using wide band gap materials. The literature data associate low PCEs with the recombination at the HTL/perovskite interfaces. Indeed, narrowing of bandgap HTM enhances the efficiency losses in solar cells due to the interface recombination processes.

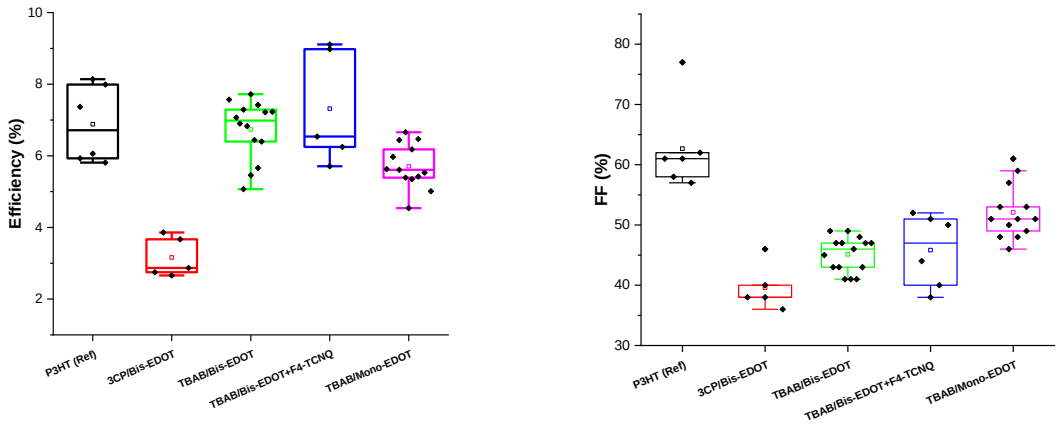

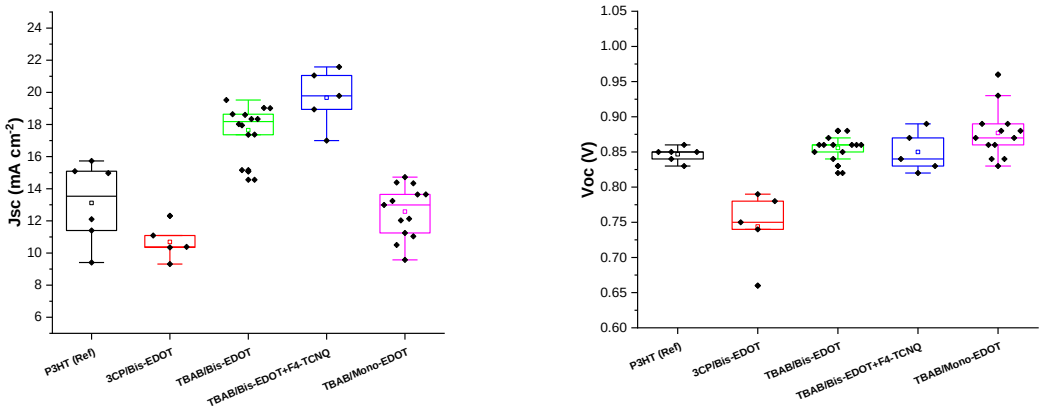

Figure 9 n-i-p PSC device PV parameter statistics of FTO/c-TiO_2/mTiO_2/perovskite/TBABr/**5a'**/Au.

3. Conclusion

In summary, we have demonstrated a facile protocol for the synthesis of indophenine dyes from readily accessible isatin derivatives. A protocol that is highly selective and allows for a very clean reaction, high yields, isomer-free materials and avoids any complex purification issues. Furthermore, this new approach allows access to end-group and core-tunable quinoidal molecules and the modulation of their optoelectronic properties by either engineering of the π-bridge or the end-group. These end-group functionalized indophenine quinoidal molecules can also be used as building blocks for the fabrication of novel conjugated systems. Spectroscopic, electrochemical and electrical measurements proved that these materials are suitable for being as an HTM in PSC devices.

Acknowledgements

This work benefited from the support of EDF in the framework of the research and teaching Chair «Sustainable energies » at Ecole polytechnique. A.Y. and M. F. thank ANR-16-CE07-0024 (GATE), R.S. thanks the China Scholarship Council for a PhD fellowship (No.201808070090). The confocal optical microscopy characterization and angle contact measurements, part of this work benefited through the use of PLATINE platform, from the support of the Ecole Polytechnique fund raising –Smart Environments: Nanosensors and Nanoreliability Initiative

References

(1) Huang, J.; Yu, G. Recent progress in quinoidal semiconducting polymers: structural evolution and insight. *Materials Chemistry Frontiers* **2021,** *5* (1), 76-96, DOI: 10.1039/d0qm00509f.
(2) Zhang, C.; Zhu, X. n-Type quinoidal oligothiophene-based semiconductors for thin-film transistors and thermoelectrics. *Advanced Functional Materials* **2020,** *30* (31), 2000765, DOI: 10.1002/adfm.202000765.
(3) Tormos, G. V.; Belmore, K. A.; Cava, M. P. The indophenine reaction revisited. Properties of a soluble dialkyl derivative. *Journal of the American Chemical Society* **1993,** *115* (24), 11512-11515, DOI: 10.1021/ja00077a057.
(4) Kim, Y.; Hwang, H.; Kim, N. K.; Hwang, K.; Park, J. J.; Shin, G. I.; Kim, D. Y. pi-Conjugated Polymers Incorporating a Novel Planar Quinoid Building Block with Extended Delocalization and High Charge Carrier Mobility. *Adv Mater* **2018,** *30* (22), 1706557, DOI: 10.1002/adma.201706557.

(5) Guo, K.; Wu, B.; Jiang, Y.; Wang, Z.; Liang, Z.; Li, Y.; Deng, Y.; Geng, Y. Synthesis of an isomerically pure thienoquinoid for unipolar n-type conjugated polymers: effect of backbone curvature on charge transport performance. *Journal of Materials Chemistry C* **2019,** *7* (33), 10352-10359, DOI: 10.1039/C9TC03556G.
(6) Ren, L.; Fan, H.; Huang, D.; Yuan, D.; Di, C.-a.; Zhu, X. Dithienoindophenines: p-Type Semiconductors Designed by Quinoid Stabilization for Solar-Cell Applications. *Chemistry – A European Journal* **2016,** *22* (48), 17136-17140, DOI: 10.1002/chem.201603112.
(7) Deng, Y.; Sun, B.; He, Y.; Quinn, J.; Guo, C.; Li, Y. Thiophene-S, S-dioxidized Indophenine: A Quinoid-Type Building Block with High Electron Affinity for Constructing n-Type Polymer Semiconductors with Narrow Band Gaps. *Angewandte Chemie International Edition* **2016,** *55* (10), 3459-3462, DOI: 10.1002/anie.201508781.
(8) Deng, Y.; Quinn, J.; Sun, B.; He, Y.; Ellard, J.; Li, Y. Thiophene-S, S-dioxidized indophenine (IDTO) based donor–acceptor polymers for n-channel organic thin film transistors. *RSC advances* **2016,** *6* (41), 34849-34854, DOI: 10.1039/C6RA03221D.
(9) Pappenfus, T. M.; Helmin, A. J.; Wilcox, W. D.; Severson, S. M.; Janzen, D. E. ProDOT-Assisted Isomerically Pure Indophenines. *The Journal of Organic Chemistry* **2019,** *84* (17), 11253-11257, DOI: 10.1021/acs.joc.9b01525.
(10) Hwang, K.; Lee, M.-H.; Kim, J.; Kim, Y.-J.; Kim, Y.; Hwang, H.; Kim, I.-B.; Kim, D.-Y. 3,4-Ethylenedioxythiophene-Based Isomer-Free Quinoidal Building Block and Conjugated Polymers for Organic Field-Effect Transistors. *Macromolecules* **2020,** *53* (6), 1977-1987, DOI: 10.1021/acs.macromol.9b02237.
(11) Sun, Y.; Zhang, Y.; Ran, Y.; Shi, L.; Zhang, Q.; Chen, J.; Li, Q.; Guo, Y.; Liu, Y. Methoxylation of quinoidal bithiophene as a single regioisomer building block for narrow-bandgap conjugated polymers and high-performance organic field-effect transistors. *Journal of Materials Chemistry C* **2020**, DOI: 10.1039/D0TC02199G.
(12) Kim, Y.; Hwang, H.; Kim, N.-K.; Hwang, K.; Park, J.-J.; Shin, G.-I.; Kim, D.-Y. π-Conjugated Polymers Incorporating a Novel Planar Quinoid Building Block with Extended Delocalization and High Charge Carrier Mobility. *Advanced Materials* **2018,** *30* (22), 1706557, DOI: https://doi.org/10.1002/adma.201706557.
(13) Steck, C.; Franckevičius, M.; Zakeeruddin, S. M.; Mishra, A.; Bäuerle, P.; Grätzel, M. A–D–A-type S,N-heteropentacene-based hole transport materials for dopant-free perovskite solar cells. *Journal of Materials Chemistry A* **2015,** *3* (34), 17738-17746, DOI: 10.1039/C5TA03865K.
(14) Rodríguez-Seco, C.; Cabau, L.; Vidal-Ferran, A.; Palomares, E. Advances in the Synthesis of Small Molecules as Hole Transport Materials for Lead Halide Perovskite Solar Cells. *Accounts of Chemical Research* **2018,** *51* (4), 869-880, DOI: 10.1021/acs.accounts.7b00597.
(15) Tokunaga, T.; Hume, W. E.; Umezome, T.; Okazaki, K.; Ueki, Y.; Kumagai, K.; Hourai, S.; Nagamine, J.; Seki, H.; Taiji, M.; Noguchi, H.; Nagata, R. Oxindole Derivatives as Orally Active Potent Growth Hormone Secretagogues. *Journal of Medicinal Chemistry* **2001,** *44* (26), 4641-4649, DOI: 10.1021/jm0103763.
(16) Mazaki, Y.; Murata, S.; Kobayashi, K. Thermal and photochemical formation of quinonoid derivatives of condensed polythiophenes and their spectral properties. *Tetrahedron letters* **1991,** *32* (34), 4367-4370, DOI: 10.1016/S0040-4039(00)92172-5.
(17) Wang, J.; Xu, X.; Phan, H.; Herng, T. S.; Gopalakrishna, T. Y.; Li, G.; Ding, J.; Wu, J. Stable Oxindolyl-Based Analogues of Chichibabin's and Muller's Hydrocarbons. *Angew Chem Int Ed Engl* **2017,** *56* (45), 14154-14158, DOI: 10.1002/anie.201708612.
(18) Wang, D.; Ying, W.; Zhang, X.; Hu, Y.; Wu, W.; Hua, J. Near-infrared absorbing isoindigo sensitizers: Synthesis and performance for dye-sensitized solar cells. *Dyes and Pigments* **2015,** *112*, 327-334, DOI: 10.1016/j.dyepig.2014.07.017.
(19) Han, J.; Chen, Y.; Chen, W.; Yu, C.; Song, X.; Li, F.; Wang, Y. High Performance Small-Molecule Cathode Interlayer Materials with D-A-D Conjugated Central Skeletons and Side Flexible Alcohol/Water-Soluble Groups for Polymer Solar Cells. *ACS Appl Mater Interfaces* **2016,** *8* (48), 32823-32832, DOI: 10.1021/acsami.6b10900.
(20) Miozzo, L.; Battaglini, N.; Braga, D.; Kergoat, L.; Suspène, C.; Yassar, A. Synthesis and characterization of all-conjugated copolymers of 3-hexyl-thiophene and EDOT by grignard metathesis

polymerization. *Journal of Polymer Science Part A: Polymer Chemistry* **2012,** *50* (3), 534-541, DOI: https://doi.org/10.1002/pola.25062.
(21) Willker, W.; Leibfritz, D. Determination of heteronuclear long-range H, X coupling constants from gradient-selected HMBC spectra. *Magnetic resonance in chemistry* **1995,** *33* (8), 632-638, DOI: 10.1002/mrc.1260330804.
(22) Deng, Y.; Quinn, J.; Sun, B.; He, Y.; Ellard, J.; Li, Y. Thiophene-S,S-dioxidized indophenine (IDTO) based donor–acceptor polymers for n-channel organic thin film transistors. *RSC Advances* **2016,** *6* (41), 34849-34854, DOI: 10.1039/C6RA03221D.
(23) Jayakannan, M.; Lou, X.; van Dongen, J. L.; Janssen, R. A. Synthesis of regioregular poly (3-octylthiophene) s via Suzuki polycondensation and end-group analysis by matrix-assisted laser desorption/ionization time-of-flight mass spectrometry. *Journal of Polymer Science Part A: Polymer Chemistry* **2005,** *43* (7), 1454-1462, DOI: 10.1002/pola.20618.
(24) Pappenfus, T. M.; Raff, J. D.; Hukkanen, E. J.; Burney, J. R.; Casado, J.; Drew, S. M.; Miller, L. L.; Mann, K. R. Dinitro and quinodimethane derivatives of terthiophene that can be both oxidized and reduced. Crystal structures, spectra, and a method for analyzing quinoid contributions to structure. *The Journal of organic chemistry* **2002,** *67* (17), 6015-6024, DOI: 10.1021/jo025572b.
(25) Takahashi, T.; Matsuoka, K.-i.; Takimiya, K.; Otsubo, T.; Aso, Y. Extensive Quinoidal Oligothiophenes with Dicyanomethylene Groups at Terminal Positions as Highly Amphoteric Redox Molecules. *Journal of the American Chemical Society* **2005,** *127* (25), 8928-8929, DOI: 10.1021/ja051840m.
(26) Casado, J. Para-Quinodimethanes: A Unified Review of the Quinoidal-Versus-Aromatic Competition and its Implications. *Top Curr Chem (Cham)* **2017,** *375* (4), 73, DOI: 10.1007/s41061-017-0163-2.
(27) Seki, K. Ionization Energies of Free Molecules and Molecular Solids. *Molecular Crystals and Liquid Crystals Incorporating Nonlinear Optics* **1989,** *171* (1), 255-270, DOI: 10.1080/00268948908065800.
(28) Frank, K. H.; Yannoulis, P.; Dudde, R.; Koch, E. E. Unoccupied molecular orbitals of aromatic hydrocarbons adsorbed on Ag(111). *The Journal of Chemical Physics* **1988,** *89* (12), 7569-7576, DOI: 10.1063/1.455720.
(29) Kirihata, H.; Uda, M. Externally quenched air counter for low-energy electron emission measurements. *Review of Scientific Instruments* **1981,** *52* (1), 68-70, DOI: 10.1063/1.1136448.
(30) Sworakowski, J. How accurate are energies of HOMO and LUMO levels in small-molecule organic semiconductors determined from cyclic voltammetry or optical spectroscopy? *Synthetic Metals* **2018,** *235*, 125-130, DOI: https://doi.org/10.1016/j.synthmet.2017.11.013.
(31) Scholz, F. *Electroanalytical methods*, Springer: 2010; Vol. 1.
(32) Willems, R. E. M.; Weijtens, C. H. L.; de Vries, X.; Coehoorn, R.; Janssen, R. A. J. Relating Frontier Orbital Energies from Voltammetry and Photoelectron Spectroscopy to the Open-Circuit Voltage of Organic Solar Cells. *Advanced Energy Materials* **2019,** *9* (10), 1803677, DOI: https://doi.org/10.1002/aenm.201803677.
(33) Ponce Ortiz, R.; Casado, J.; Rodríguez González, S.; Hernández, V.; López Navarrete , J. T.; Viruela, P. M.; Ortí , E.; Takimiya, K.; Otsubo, T. Quinoidal Oligothiophenes: Towards Biradical Ground-State Species. *Chemistry – A European Journal* **2010,** *16* (2), 470-484, DOI: https://doi.org/10.1002/chem.200902037.
(34) Du, T.; Xu, W.; Daboczi, M.; Kim, J.; Xu, S.; Lin, C.-T.; Kang, H.; Lee, K.; Heeney, M. J.; Kim, J.-S.; Durrant, J. R.; McLachlan, M. A. p-Doping of organic hole transport layers in p–i–n perovskite solar cells: correlating open-circuit voltage and photoluminescence quenching. *Journal of Materials Chemistry A* **2019,** *7* (32), 18971-18979, DOI: 10.1039/C9TA03896E.
(35) Hwang, H.; Khim, D.; Yun, J.-M.; Jung, E.; Jang, S.-Y.; Jang, Y. H.; Noh, Y.-Y.; Kim, D.-Y. Quinoidal Molecules as a New Class of Ambipolar Semiconductor Originating from Amphoteric Redox Behavior. *Advanced Functional Materials* **2015,** *25* (7), 1146-1156, DOI: https://doi.org/10.1002/adfm.201402758.
(36) Wang, X.; Ederth, T.; Inganäs, O. In Situ Wilhelmy Balance Surface Energy Determination of Poly(3-hexylthiophene) and Poly(3,4-ethylenedioxythiophene) during Electrochemical Doping−Dedoping. *Langmuir* **2006,** *22* (22), 9287-9294, DOI: 10.1021/la061606p.

(37) Oswald, J.; Beretta, D.; Stiefel, M.; Furrer, R.; Romio, A.; Mansour, M. D.; Vuillaume, D.; Calame, M. Charge Transport Across Au–P3HT–Graphene van der Waals Vertical Heterostructures. *ACS Applied Materials & Interfaces* **2022,** *14* (42), 48240-48249, DOI: 10.1021/acsami.2c13148.
(38) Marin-Beloqui, J. M.; Hernández, J. P.; Palomares, E. Photo-induced charge recombination kinetics in MAPbI3−xClx perovskite-like solar cells using low band-gap polymers as hole conductors. *Chemical Communications* **2014,** *50* (93), 14566-14569, DOI: 10.1039/C4CC06338D.